Walnut shell biochar supported TiO$_2$–g-C$_3$N$_4$ heterojunction photocatalyst for solar photocatalytic degradation of congo red

Abhishek Patil[1] · Neelancherry Remya[1] · Naresh Singhal[2] · Brajesh Kumar Dubey[3]

Abstract

Biochar has multiple applications, one of which is to act as a supporting material for catalysts in various treatment processes. Solar-light-driven photocatalysis is one of the efficient treatment methods for textile industry wastewaters, typically containing recalcitrant organic compounds such as dyes. It offers a convenient, simple, cost-effective and efficient method of radical generation for pollutant degradation using solar energy. The present study investigates the application of walnut shell biochar (WSB) to immobilize the solar light-responsive TiO$_2$–g-C$_3$N$_4$ heterojunction photocatalyst for congo red (CR) dye degradation. Different facile and modified methods for the production of the heterojunction photocatalysts such as the sol-gel method (with and without some modifications), ultrasonication and single-step calcination methods. These samples were then characterized for surface morphology, crystallinity, elemental composition and photoactivity. About 60% degradation efficiency could be achieved for the CR solution with an initial concentration of 10 mg/L and a catalyst dosage of 1 g/L at the end of 3 h irradiation. It was observed that photocatalysis proved to be a major removal mechanism than adsorption by biochar, but the WSB assisted in the easy separation of the photocatalyst from the dye solution after the treatment. The study concluded that the photocatalysts synthesized using facile methods can be effectively employed for CR degradation under solar light irradiation.

1 Introduction

Rapid growth in population, industrialization and urban development leads to an increase in water and energy demand. The limited availability of fresh water and the increasing production of wastewater necessitates the development of novel methods for effective wastewater treatment, such that it can be reused further to quench the demand. On the other hand, the textile industry is reported to be one of the major water-consuming industries requiring 150–933 L per kg of product [1], generating around 200–350 m^3 of effluent per ton of finished product [2]. Several dyes contain nearly 40% organically bounded chlorine, which is a carcinogen, and other heavy metals. Their colouring property is imparted by the presence of chromophores with azo bonds. There are other compounds containing hydrosulphide groups in textile effluents as well, which are responsible for the decrease in oxygen content in water bodies. Such effluents also affect the aquatic ecosystem by causing hindrance in the penetration of Solar-light [3]. The presence of recalcitrant organic compounds like dyes, detergents, etc. in these wastewater leads to inefficient treatment capability of conventional municipal sewage treatment plants involving biological treatment methods [4]. Many physiochemical treatments like adsorption, filtration, coagulation, and advanced oxidation processes (AOPs) were examined for dye removal from wastewater. AOPs aim at the complete oxidation of organic contaminants (mineralization) or their conversion to end products that are lesser toxic in nature, owing to their non-selective pathway, higher oxidation potential for pollutant mineralization and higher reaction rates [5]. Among various AOPs, photocatalysis is considered desirable for the

✉ Neelancherry Remya
  remya@iitbbs.ac.in

1   School of Infrastructure, Indian Institute of Technology Bhubaneswar, Argul 752050, Odisha, India

2   Department of Civil and Environmental Engineering, The University of Auckland, Private Bag 92019, Auckland 1142, New Zealand

3   Department of Civil Engineering, Indian Institute of Technology Kharagpur, Kharagpur, India

treatment of dye-laden effluent. This process is a sustainable, cost-effective and energy-efficient technology that can be applied to wastewaters with low biodegradability, high levels of pollution as well as complexity [6]. It is an oxidation-reduction reaction carried out by reactive oxidizing species that are formed due to the generation of photon-activated electrons and holes from the surface of the photocatalysts [7]. While UV light can be used as a source of light for photo-excitation of photocatalysts, there are certain solar-light responsive materials that can harness the solar light and get activated for participating in photochemical reactions for decontamination of water, thus making the process cost-effective [8].

In recent times, the application of nanotechnology in the field of water and wastewater treatment is gaining tremendous attention and scope for research. It is mainly adopted for the remediation of contaminated water and detection as well as prevention of water pollution [9]. Generally, nanomaterials such as titanium dioxide (TiO_2) are used as photocatalysts for water remediation by photocatalysis. TiO_2 has gained significant attention over the past few years because of its advantages: low toxicity, high optical reactivity, cost-effectiveness, high surface area to volume ratio, a strong positive valence band (VB) potential etc. [10, 11]. However, the drawbacks that limit the application of TiO_2 and other single-component photocatalysts are low photocatalytic efficiency due to rapid charge recombination, wide band gap and insufficient redox potentials [12]. Modification techniques such as doping with metallic/non-metallic elements, defect structure generation, coupling with noble metals, heterojunction formation, etc. are adopted to overcome these drawbacks [5].

Constructing heterojunctions between different semiconductors is an efficient method of enhancing the photocatalytic activity of the semiconductors. A heterojunction is generally formed by combining two semiconductors and/or metals depending on the band structure or alignment. This allows the enhancement of photocatalytic activity, effective charge separation and redox potential [13]. Graphitic carbon nitride ($g-C_3N_4$) is gaining significant attention among metal-free photocatalysts because of its low cost and facile synthesis and narrow band gap of 2.7 eV that allows visible light excitation [14]. Since it possesses a strong negative conduction band (CB) potential, it can serve as a reduction photocatalyst while preparing a heterojunction. There are certain heterojunctions developed using $g-C_3N_4$, amongst which $TiO_2–g-C_3N_4$ is researched widely for its better photocatalytic ability under visible light conditions when compared with TiO_2 and $g-C_3N_4$ alone. It is associated with the enhancement of photo-generated electron-hole pair separation effectiveness in the $TiO_2–g-C_3N_4$ heterojunction [15].

The photoactivity of a photocatalyst can be enhanced by increasing its surface area, which is achieved when it is used in fine, powdered form. However, this leads to difficulty in its post-treatment separability from the effluent. To overcome this drawback, photocatalysts can be immobilized onto appropriate support materials such as granular activated carbon, glass fibres, quartz, silica, etc. [16]. Biochar is an environmentally friendly and sustainable carbon substance obtained through pyrolysis of bio-based products. The recent advancement of technology involves the usage of Microwaves for the thermochemical conversion process instead of conventional pyrolysis, providing better product yield due to rapid, uniform and selective heating. Additionally, Microwave-Assisted Pyrolysis (MAP) also overcomes the major disadvantages of conventional pyrolysis such as low heating rate, greenhouse gas emissions, and large carbon footprint [17]. Biochar tend to have a large specific surface area, stratified pore structure, thermal and chemical stability, electrical conductivity and functional groups and thereby can be used for various environmental applications [18]. Apart from being used as a fuel replacement, biochar can also be useful as an adsorbent for pollutant removal in wastewater treatment, soil conditioner, fine chemical production, fertilizer to improve crop yield, support material for catalytic activities etc. [19]. The presence of tunable surface groups and the high stability of the biochar provide an ability to act as an effective supporting platform for the production of biochar-supported photocatalysts [20]. Recently biochar from various agricultural residues like rice husk, softwood pellets, corn stalks, coconut shells, and raisin leaves have been used as support material for photocatalytic treatment processes [21].

The objective of this present study is to explore the application of walnut shell biochar (WSB) obtained from MAP as a support material for photocatalytic dye degradation using $TiO_2–g-C_3N_4$ heterojunction photocatalyst. The heterojunction photocatalyst between TiO_2 and $g-C_3N_4$ was prepared by adopting various cost-effective, easy and convenient synthesis methods such as the modified sol-gel method, ultrasonication, and single-step calcination. The effect of heterojunction formation on the surface morphology, crystallinity, band-gap modification, surface area and elemental composition of the photocatalyst was investigated. Further, the synthesized heterojunction photocatalyst was supported on the WSB and employed for the degradation of congo red (CR) dye under solar light radiation.

2 Materials and methodology

2.1 Chemicals

Walnut shell feedstock for biochar preparation was obtained from the local market at Bhubaneswar, India. Titanium (IV) isopropoxide was procured from Himedia,

India whereas commercial pure titanium (IV) dioxide powder was purchased from Merck, India. Analytical grade urea (99%) was purchased from TM media, India and hydrogen peroxide (H_2O_2, 30%) was obtained from Avra Synthesis, Hyderabad, India.

2.2 Preparation of walnut shell biochar (WSB)

WSB was prepared in a batch-mode microwave pyrolysis reactor operating at a frequency of 2,450 MHz and maximum output power of 1000 W. The reactor was purged with nitrogen gas before and during the pyrolysis process to provide inert conditions throughout the process. A certain amount of walnut shell feedstock was washed, dried, shredded and pyrolyzed in MAP reactor for a duration of 30 min at 800W power. The biochar obtained was cooled to room temperature and then acid-washed to remove any impurities before using it for photocatalyst immobilization. The biochar sample was pre-treated by washing it under tap water several times and then immersing it in 0.01 M H_2SO_4 solution in an orbital shaker overnight. This was later followed by rinsing with tap water again and keeping in a hot air oven overnight. The elemental composition of the biochar sample was done using elemental analyser (Euro Vector EA3000).

2.3 Synthesis of TiO₂–g-C₃N₄ heterojunction catalyst

Simple thermal condensation of urea was adopted to obtain g-C_3N_4. 10 g of urea was taken in a crucible, covered with a lid and annealed at 550 °C for 4 h after placing it in a muffle furnace with a heating rate of 2.2 °C/min approximately. After the thermal condensation, the crucible was allowed to cool down to room temperature and yellow-colored powder of g-C_3N_4 was finally obtained, which was used without any further modifications.

Five different samples of the required heterojunction photocatalyst were prepared by adopting different synthesis routes. In sol-gel method, a sol of TiO_2 was obtained by adding 5 mL of titanium (IV) isopropoxide drop-wise to a solution of 250 mL of deionized water with 50 mL absolute ethanol and 1 mL HCl (37%). To this sol, g-C_3N_4 was added to maintain the ratio of 1:2 for TiO_2 and g-C_3N_4 respectively on weight basis. The mixture was then homogenized by magnetic stirring for 30 min at 400 rpm. The mixture was kept in a water bath for 2 h at 80 °C, followed by cooling to room temperature. Later, it was dried and then calcined at 550 °C for 2 h, further cooled down and the powdered sample obtained is named SG. The next two samples were prepared using the ultrasonication-assisted sol-gel method. Similar to the previous method, the homogenized mixture of TiO_2 sol with g-C_3N_4 was prepared. It was then subjected to ultrasonication for 60 min at 45% amplitude and 0.3 duty

cycle. After that, the solution was cooled down to room temperature and allowed to evaporate in a hot-air oven at 105 °C. The solid sample obtained was finally calcined at 550 °C for 2 h in a muffle furnace to obtain the second photocatalyst sample, named USG-MF. The third sample was prepared similarly, the only difference being the type of final heat treatment given to the evaporated sample. A similar procedure was carried out to obtain an ultrasonicated sample as followed for the second sample. However, the solid sample obtained after evaporation was then heated in a microwave reactor for 10 min with 500 W power and the temperature set was 550 °C. The finally obtained third sample was named USG-MW.

Another sample was prepared by adopting the ultrasonication method. 50 mg of g-C_3N_4 and 100 mg of TiO_2 powder were added to 100 mL deionized water, to which 50 mL ethanol was later added. After stirring it for 10 min, the suspension was ultrasonicated at 400 W with 45% amplitude and 0.3 duty cycle for 1 h. The sonicated solution was then stirred for 1 h and later allowed to evaporate at 100 °C. A white powder obtained after evaporation was then placed in a crucible covered with a lid and calcined at 550 °C for 2 h in a muffle furnace. The final photocatalyst obtained was then labelled US.

For the synthesis of the photocatalysts sample using single-step calcination method, 6 g of urea was added to 50 mL of deionized water to obtain a clear solution after mixing. To this, 0.2 g of commercial TiO_2 was added. The suspension was then magnetically stirred at 300 rpm for 2 h and later evaporated at 100 °C to obtain a white residue. This residue is then put in a crucible, covered with a lid and placed in a muffle furnace for calcination at 550 °C for 2 h. Finally, a white powdered photocatalyst sample was obtained and labelled SSC.

2.4 Synthesis of WSB supported TiO₂–g-C₃N₄ heterojunction photocatalyst

For immobilizing the photocatalysts, a simple solvent deposition method was used. A mixture of ethanol and water (80:20) was used as an immersion solution for this purpose. The coating process by dipping the WSB in immersion solution containing powdered photocatalyst and taking it out was followed by air-drying and such multiple cycles were followed for better coating. Finally, the coated sample was kept in an oven overnight for drying.

2.5 Characterization of photocatalyst

The photocatalysts were characterized and analyzed for understanding their surface morphology, elemental composition, crystallinity and effect of band gap modification. Morphology and elemental distribution of unsupported

photocatalyst were analyzed with the help of scanning electron microscopy (SEM) (MERLIN compact, Carl Zeiss) coupled with electron dispersive spectroscopy (EDS) (51XMX 1004, Oxford Instruments). X-ray dispersive spectroscopy (XRD) (D8 Advance, Bruker) was adopted for analyzing the crystallinity of samples. The effect of heterojunction modification on band gap for visible light excitation was analyzed using a UV-visible spectrophotometer (Analytical ® Instruments Limited). All the above characterizations were carried out before supporting the photocatalysts on the biochar. Fourier Transform Infrared (FTIR) spectroscopy was performed to analyse and understand the chemical bonding of components of WSB supported heterojunction photocatalyst. The electrochemical impedance spectroscopy (EIS) of the unsupported as well as supported photocatalyst samples was carried out to evaluate the transfer of charge carriers and the separation efficiency [22]. The elemental analysis and surface area of WSB used as support material for photocatalysis was carried out using elemental analyser (Euro Vector EA3000) and BET Analyser respectively.

2.6 Photocatalytic degradation of congo-red (CR)

The photocatalytic degradation of CR was carried out in a simple enclosed experimental setup (Fig 1), consisting of a visible-light lamp (tungsten-halogen lamp with the power 150 W and with primary emission in wavelength of 400-700 nm) for simulating solar light with the provision of an immersion well for cooling purposes. 100 mL of the CR dye solution with an initial concentration 10 mg/L was taken. Catalyst dosage was fixed to 1 g/L. All the experiments were conducted thrice and the average of these results is reported here. The residual CR concentrations were determined with the help of UV-visible spectroscopy. The recyclability of the photocatalyst was tested by separating the photocatalyst from the solution by sedimentation and filtration, followed by washing with mild acid before using it for the consecutive runs. Furthermore, the quenching of different radicals namely $^{\bullet}OH$ (Hydroxyl), $^{\bullet}O^{2-}$ (Superoxide), e^{-} (photogenerated electron), and h^{+} (photogenerated holes)

were determined using different scavengers like Salicylic acid (SA), p-benzoquinone (p-BQ), silver nitrate (AgNO$_3$), and EDTA respectively to study their effect in photocatalytic degradation [23].

2.7 Quantification of hydroxyl radical production

The hydroxyl radicals ($^{\bullet}OH$) generated as a result of activation of the photocatalyst were quantified indirectly with the help of a UV-visible light spectrophotometer by using salicylic acid (SA) as a scavenger. The initial standard concentration of SA used was 10^{-3} M and the concentrations were measured at a wavelength of 303 nm.

3 Results and discussion

3.1 Characterization of photocatalysts

3.1.1 Morphological analysis

The SEM images of the photocatalyst samples prepared using different methods as discussed before sol-gel method (SG), ultrasonication-assisted sol-gel method with microwave heat treatment (USG-MW), ultrasonication-assisted sol-gel method with muffle furnace heat treatment (USG-MF), ultrasonication method (US) and single step calcination method (SSC) are illustrated below. The sol-gel and ultrasonication-assisted sol-gel method photocatalysts were composed of particles with non-uniform and irregular shapes. The samples SG, USG and SSC were found to have continuous, mesh-like structures and as a result, it was difficult to determine the average size of the particles. US sample showed uniform-sized spherical particles with an average size of 146 nm. This can be due to effective size reduction by ultrasonication. The average size of the particles in USG-MW was around 163 nm. The SEM images of the samples are shown along with their corresponding EDS analysis image in Fig 2.

Fig. 1 (**a**) Schematic diagram, and (**b**) actual photo of the experimental setup


(a)

(b)
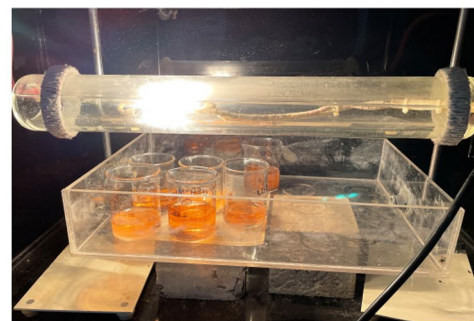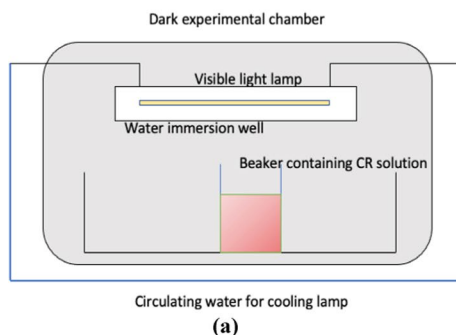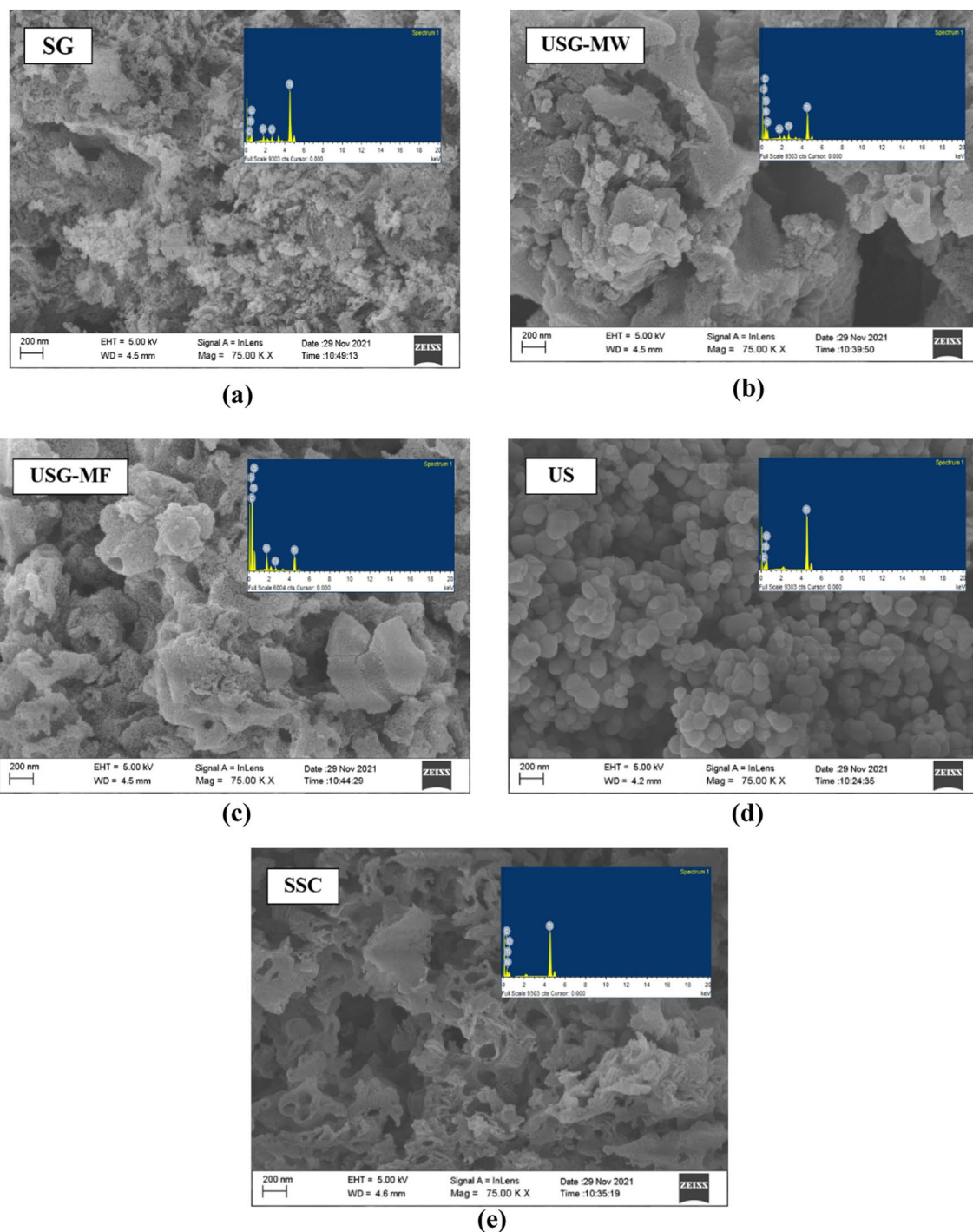
Fig. 2 SEM and EDS analysis images for photocatalysts

The specific surface area of WSB was determined to be 88.2 m^2/g, which is much greater than TiO$_2$ (6.28 m^2/g) and g-C$_3$N$_4$ (0.79 m^2/g). The surface area slightly reduced to 4.37 m^2/g for the combined TiO$_2$–g-C$_3$N$_4$ photocatalyst. The N$_2$ adsorption-desorption plot obtained through BET analysis of TiO$_2$, g-C$_3$N$_4$, and TiO$_2$–g-C$_3$N$_4$ heterojunction are given in Fig 3.

3.1.2 Elemental composition

The ultimate analysis of WSB used for supporting the photocatalyst determined the carbon (C), hydrogen (H), sulphur (S), and nitrogen (N) as 76.56%, 3.156%, 0.041%, and 2.165% respectively. WSB can facilitate the photocatalytic degradation of CR due to its higher
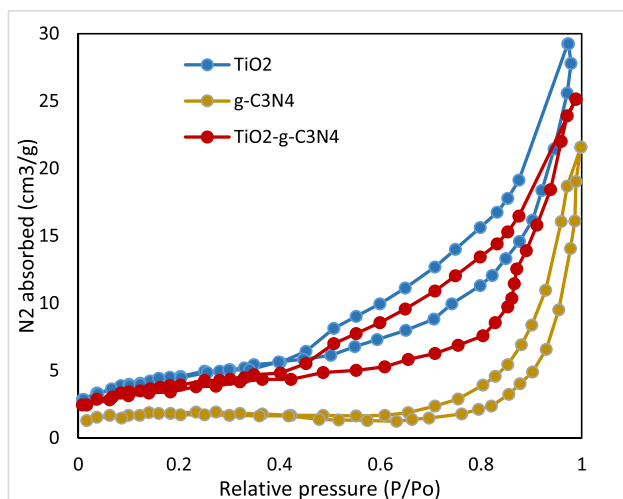
Fig. 3 N$_2$ Adsorption-desorption curve of Photocatalyst

Fig. 4 FTIR response spectrum for WSB supported photocatalyst

carbon content and surface area. The elemental composition of the photocatalysts before immobilizing them was determined using EDS coupled with SEM. Surprisingly, it was seen that nitrogen was not detected in all samples, as it should have been since g-C$_3$N$_4$ is an integral component of the system. This can indicate that the g-C$_3$N$_4$ sample used might have been prepared by incomplete thermal condensation of urea or some issue due to temperature change could have resulted in unwanted reaction and thus the nitrogen loss. The EDS analysis images and the elemental composition of the samples focusing only on Ti, O, N and C are illustrated in Table 1. The chemical bonding of components of WSB supported heterojunction photocatalyst were analysed using FTIR spectroscopic results shown in the Fig 4. The small peak observed in the range of 3000-3500 cm^{-1} could be possibly attributed to the influence of water adsorbed onto the sample. The peaks obtained in the range of 1200-1700 cm^{-1} could be attributed to the aromatic C-N bond present in g-C$_3$N$_4$, whereas the major peak observed at 800 cm^{-1} can be associated with Ti-O-Ti and Ti-O stretching modes due to TiO$_2$.

3.1.3 Crystallinity analysis

The crystallinity and phases of different photocatalysts were analyzed with the help of XRD and the spectra within the diffraction angle $10° < 2θ < 80°$ obtained for them are illustrated in Fig 5. The diffraction peaks observed here for all the samples lie closely around 25°, 39°, 48°, 55°, 62°, 70° and 76° in general, all of which correspond to the diffractive crystal faces of anatase TiO$_2$, thus confirming the presence of anatase phase TiO$_2$.

3.1.4 Band gap modification

Full wavelength scan was performed with the help of UV-Visible spectrophotometer for all the photocatalysts to analyze the effect of heterojunction formation on band gap modification. The normalized spectra for the photocatalysts show the absorbance peaks in the visible light region, possibly because of the band gap reduction due to heterojunction formation (Fig 6). Furthermore, the energy band gap was calculated by considering the wavelength corresponding to the observed peak absorbance in the visible light region

Table 1 Elemental composition of different samples

Sample	Weight (%)				Atomic (%)			
	Ti	O	C	N	Ti	O	C	N
SG	46.10	2.01	9.06	-	21.86	1.29	17.13	-
USG-MW	17.64	27	23.16	29.56	5.96	27.33	31.23	34.18
USG-MF	25.76	15.87	44.03	-	10.04	14.45	34.56	-
US	48.94	42.59	8.47	-	23.28	60.66	16.06	-
SSC	46.78	24.68	16.43	12.11	20.55	32.46	28.79	18.20

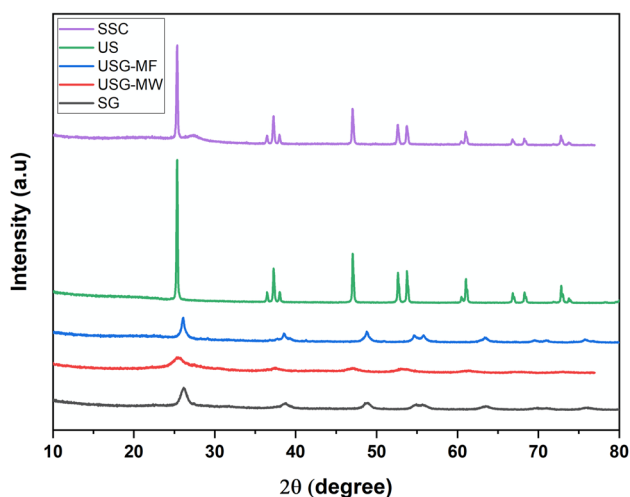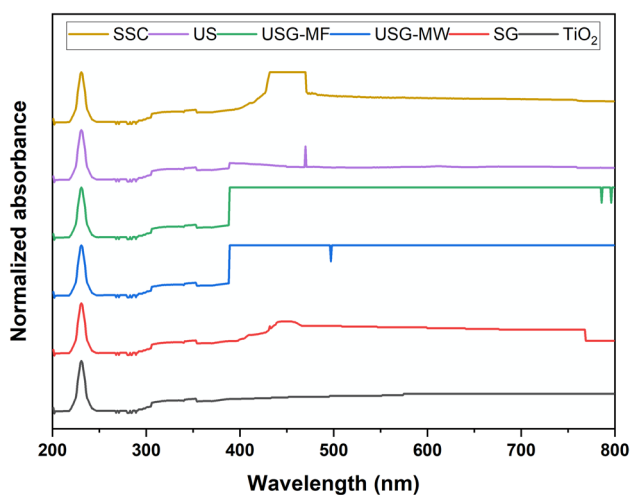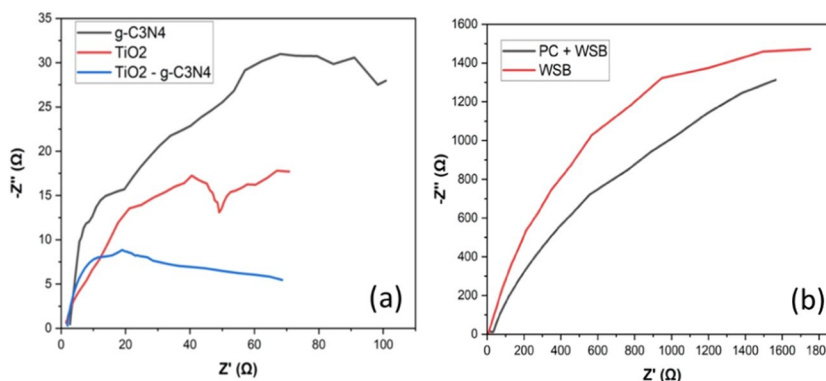**Fig. 5** XRD spectra of photocatalysts

Fig. 6 UV-visible spectra for different photocatalysts

using energy equation of quantum mechanics. The band gap followed the order of US (2.64 eV) < SSC (2.76 eV) < SG (2.78 eV) < USG-MW (3.18 eV) < USG-MF (3.19 eV) <

TiO_2 (5.41 eV). The absorbance peak for SSC was observed to be scattered along the solar light wavelength range with an average energy band gap of 2.76 eV. It can be inferred that the formation of heterojunction TiO_2–g-C_3N_4 lead to the reduction in energy band gap by circa 49% when compared to TiO_2 alone. This can confirm the visible light responsiveness of the synthesized photocatalysts, thus indicating their suitability for solar light-assisted photocatalysis.

3.1.5 Transfer of charge carriers

The electrochemical impedance spectroscopy (EIS) was carried out to understand the kinetic behaviour of charge separation and transfer. The results of EIS are represented in the form of EIS Nyquist plots, which represent the real component of the complex impedance on X-axis and the negative of the imaginary component of the complex impedance on Y-axis. The radius of the arcs obtained for photocatalysts signifies its efficiency of charge separation and transfer. The smaller the arc radius, more efficient is separation of electrons and holes, indicating their reduced recombination due to lower charge transfer resistance and thus, enhanced photoactivity of the photocatalyst. The EIS Nyquist plot for TiO_2, g-C_3N_4 and TiO_2–g-C_3N_4 is shown in Fig. 7-a. The radii of the arcs of these corresponding samples observed are in the order: g-C_3N_4 > TiO_2 > TiO_2–g-C_3N_4. Thus, it can be confirmed that the charge separation of TiO_2–g-C_3N_4 is significantly increased as compared to its individual photocatalyst components TiO_2 and g-C_3N_4 and therefore it can be addressed that the heterojunction photocatalyst can demonstrate better photocatalytic performance. Similarly, the EIS Nyquist plot (fig. 7-b) for supported heterojunction photocatalyst sample and biochar sample show the smaller radius of arc for the WSB supported photocatalyst than the WSB support material.

3.2 Photocatalytic experiment for CR degradation

The photocatalytic activity of the photocatalysts was compared based on CR dye removal efficiency (Fig 8). The unsupported photocatalysts (US and SSC) were

Fig. 7 (**a**) EIS Nyquist plot for photocatalyst components and (**b**) EIS Nyquist plot for WSB supported heterojunction photocatalyst
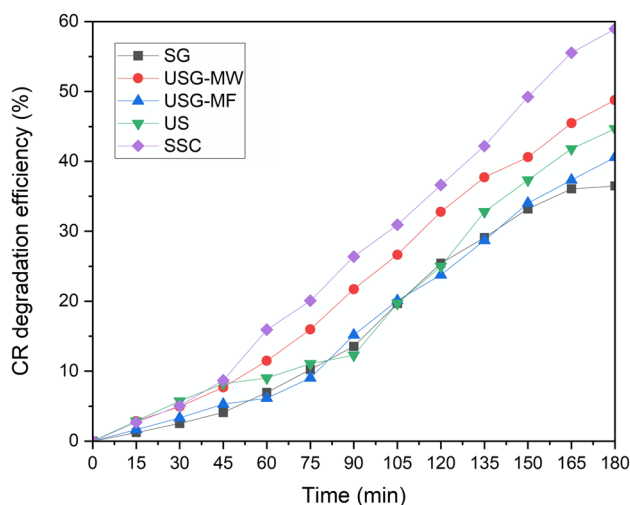
Fig. 8 Comparison of CR dye degradation efficiencies of different photocatalysts

Fig. 9 Sorption studies for CR removal by biochar and photocatalyst

immobilized onto WSB using the solvent deposition method before the experiment. Further, the two photocatalyst samples with comparatively higher efficiencies were assessed to check if there is any further enhancement in their efficiency due to the addition of an oxidant like H_2O_2. The results obtained in both experiments are discussed below.

After 3 h of experiment, the SG sample was found to be the least effective in CR degradation (removal efficiency = 25.82 %), whereas the SSC sample demonstrated the highest efficiency of 58.89 %. US sample demonstrated a removal efficiency of 40.57%. Among the sol-gel method samples, USG-MW showed a removal efficiency of 44.67%. Lastly, USG-MF could remove 36.48% CR dye from the solution. To sum up, the samples with their CR degradation efficiencies in decreasing order are as follows: SSC > USG-MW > US > USG-MF > SG. The degradation efficiency of CR with SSC improved to 93% when the treatment by increasing the treatment time to 6 h.

Sorption studies were carried out using WSB, and unsupported TiO_2–g-C_3N_4 heterojunction photocatalyst for the removal of CR by adsorption. In case of WSB, pre-treatment of biochar was done, similar to its use before immobilization of the photocatalyst. For the initial CR concentration of 10 mg/L and adsorbent dosage of 1 g/L, the maximum removal efficiency for WSB and unsupported TiO_2–g-C_3N_4 was observed to be nearly 23% and 12.13% respectively. The adsorption equilibrium for WSB and unsupported TiO_2–g-C_3N_4 reached at 120 min and 90 min respectively. After 3 h, the biochar was filtered and dried before carrying out desorption study. The increase in CR concentration as a result of desorption is shown in Fig 9. The final CR concentration at the end of 3 h was nearly 1.5 mg/L. Desorption study of the WSB supported catalyst after CR
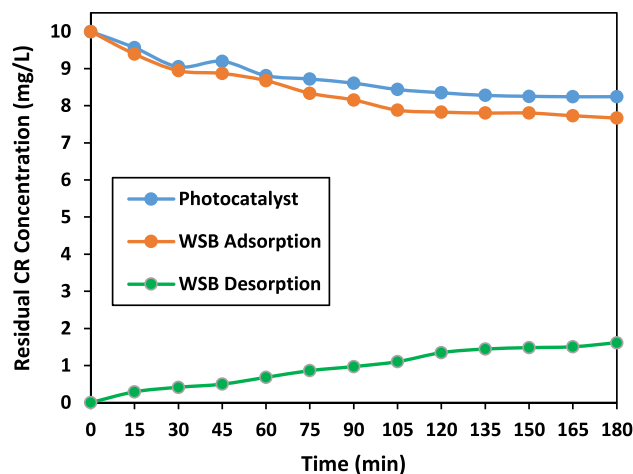
photocatalytic degradation resulted in negligible concentration of CR. These results indicate the suitability of WSB as the support material for photocatalysts and it can be inferred that adsorption by the photocatalyst plays a supportive role in the enhancement of the photoactivity as well.

3.3 Quantification of •OH by quenching of salicylic acid

An indirect method of quantification of $^{\bullet}$OH was adopted by observing the amount of salicylic acid (SA) quenched by the photocatalyst sample SSC since this sample demonstrated the best CR degradation efficiency. Two sets of experiments were conducted under visible light, with and without the addition of H_2O_2 for 3 h. The concentrations of SA were measured using a UV-spectrophotometer at a wavelength of 303 nm. It was observed that the addition of H_2O_2 resulted in a roughly 27% increase in the $^{\bullet}$OH concentration (Fig 10).

3.4 Mechanism of CR removal

To understand the mechanism behind the removal of CR under visible light-assisted photocatalysis, an experiment was carried out to assess the contribution of photolysis, photocatalysis as well as adsorption in the CR removal process. Five sets of CR solutions were taken – (i) without any addition (ii) with the addition of unsupported SSC (iii) with the addition of only biochar (iv) with the addition of SSC and (v) with the addition of only H_2O_2 (Fig 11). These solutions were then exposed to artificial visible light for 3 h to observe any significant decrease in CR concentration.

After the irradiation time, it was seen that there was no significant CR removal by mere photolysis. Adsorption did not contribute much until 2 h and then there could be a slight increase in the removal process. The mere
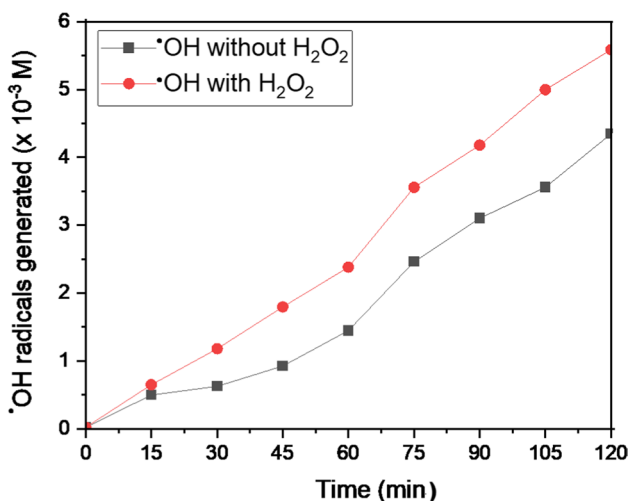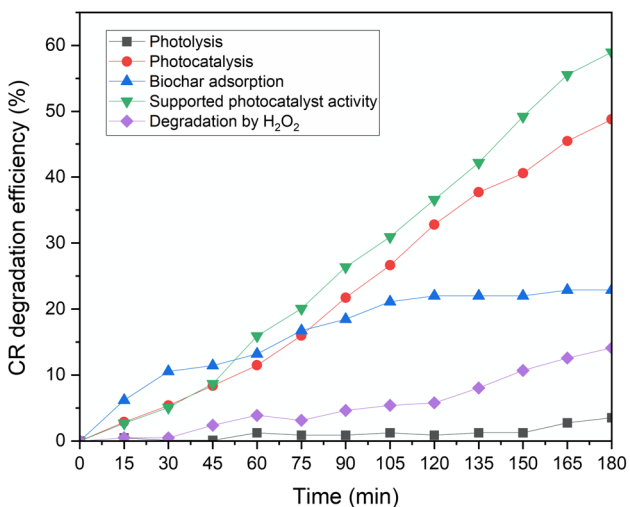
Fig. 10 Concentration profile of •OH

Fig. 11 CR degradation under different treatment methods
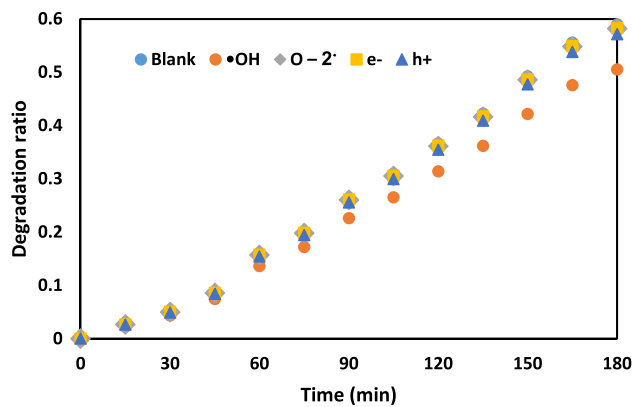

Fig. 12 Effect on CR degradation due to radical quenching
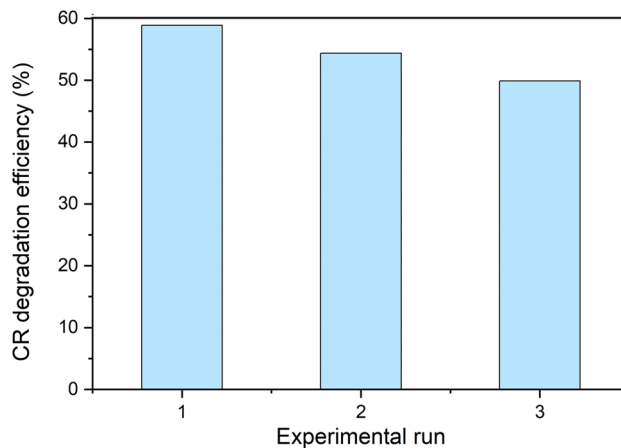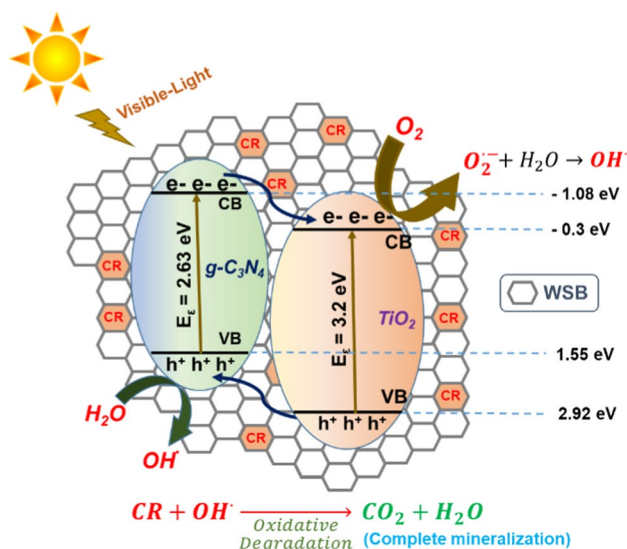

Fig. 13 Reusability test of SSC samples

3.5 Reusability test

After the first experiment time of 3 h, the biochar-supported photocatalyst was separated from the CR solution by sedimentation followed by filtration using 0.22 micron filter paper. It was then washed with a mild acid such as 0.02 N HNO$_3$. After drying it at 100 °C, the catalyst was reused for the next experimental run. The decrease in degradation efficiency of the photocatalyst over subsequent cycles is shown in Fig 13. This could have happened possibly because of adsorption of degradation by-products into the photocatalyst surface and detaching of supported photocatalyst from the biochar surface as well.

4 Proposed mechanism for dye degradation

It is hypothesised that three possible pathways are involved in the degradation of CR by photocatalysis – adsorption, photodegradation and enhanced radical formation due to

addition of H$_2$O$_2$ was not as effective as degradation by photocatalysis. The supported SSC sample showed the best removal efficiency, followed by unsupported SSC. This indicated that photocatalysis was the major contributing factor in CR removal by degrading it, while removal by adsorption was the assisting factor.

The scavenger analysis implied that the •OH played an important role in the degradation of CR. Fig 12 denotes the impact of the active species in the photocatalytic activity. The CR degradation due to the quenching of different radicals (% degradation) when compared to blank (58.9%) followed •OH (50.5%) > •O^{2-} (58.18%) > e$^-$ (58.29%) > h$^+$ (57.12%).

Fig. 14 Proposed CR degradation mechanism

oxygen supply. Biochar as a support material additionally acts as an electron sink due to its dense carbon layer, thus assisting in better electron transport and storage. The active sites on the biochar help in the adsorption of pollutants in aqueous phase to the surface, followed by effective degradation by photocatalysis. Under the simulated solar excitation, the photogenerated electrons from the conduction band of g-C_3N_4 transfers towards the conduction band of TiO_2, simultaneously the photogenerated holes from valency band of TiO_2 transfers towards the valency band of g-C_3N_4. Furthermore, the effective charge separation due to heterojunction formation helps in improved oxidation and reduction potential of the photocatalyst. During the photocatalytic dye degradation experiment, aerators were provided to keep the photocatalysts in suspension for effective photoactivity throughout the wastewater sample. The provision of additional oxygen and its reaction with the photocatalyst could also have resulted in the enhanced generation of $^\bullet O^{2-}$, which ultimately convert to $^\bullet OH$. As a result, the enhanced radical formation could have assisted in photodegradation. Hence, the CR removal is assumed to be a combined result of adsorption enhanced photodegradation. The pictorial representation of the proposed dye degradation mechanism is shown in the Fig 14.

5 Conclusion

From the obtained experiment results, it can be inferred that CR dye can be effectively degraded using biochar-based photocatalysis. The catalyst SSC showed highest degradation efficiency of 59% under simulated solar light for the initial CR concentration of 10 mg/L, catalyst dosages of 1

g/L and irradiation time of 3 h. The degradation efficiency improved to 93% when the treatment was performed for 6 h. The photocatalysis was the major mechanism behind dye degradation as compared to adsorption by biochar. CR removal due to adsorption by WSB and TiO_2–g-C_3N_4 alone was nearly 23% and 12% respectively and CR degradation by mere photocatalysis was nearly 48%. Supporting the photocatalyst onto WSB could help in enhancing its photocatalytic activity. However, the optimum dosage and optimum treatment time for the said photocatalyst were not determined in the experiment.

Declarations

References

1. Bilińska L, Gmurek M (2021) Novel trends in AOPs for textile wastewater treatment. Enhanced dye by-products removal by catalytic and synergistic actions. Water Resour Ind 26:100160. https://doi.org/10.1016/j.wri.2021.100160

2. Nidheesh PV, Divyapriya G, Titchou FE, Hamdani M (2022) Treatment of textile wastewater by sulfate radical based advanced oxidation processess. Sep Purif Technol 293:121115. https://doi.org/10.1016/j.seppur.2022.121115

3. Bhatia D, Sharma NR, Kanwar R, Singh J (2018) Physicochemical assessment of industrial textile effluents of Punjab (India). Appl Water Sci 8:83. https://doi.org/10.1007/S13201-018-0728-4

4. Ananthashankar AGR (2013) Production, Characterization and Treatment of Textile Effluents: A Critical Review. J Chem Eng Process Technol 05(01):1–18. https://doi.org/10.4172/2157-7048.1000182

5. Titchou FE et al (2021) Removal of organic pollutants from wastewater by advanced oxidation processes and its combination with membrane processes. Chem Eng Process Process Intensif 169:108631. https://doi.org/10.1016/j.cep.2021.108631

6. Shin Koe W, Wen Lee J, Chan Chong W, Ling Pang Y, Ching Sim L (2020) An overview of photocatalytic degradation: photocatalysts, mechanisms, and development of photocatalytic membrane. Environ Sci Pollut Res 27:2522–2565. https://doi.org/10.1007/s11356-019-07193-5

7. Ali N et al (2020) Photocatalytic Degradation of Congo Red Dye from Aqueous Environment Using Cobalt Ferrite Nanostructures:

Development, Characterization, and Photocatalytic Performance. Water Air Soil Pollut. https://doi.org/10.1007/s11270-020-4410-8

8. Priyanka K, Remya N, Behera M (2022) Sequential biological and solar photocatalytic treatment system for greywater treatment. Water Sci. Technol. 86(3):584–595. https://doi.org/10.2166/wst.2022.229

9. Hairom NHH et al (2021) A review of nanotechnological applications to detect and control surface water pollution. Environ Technol Innov 24:102032. https://doi.org/10.1016/j.eti.2021.102032

10. Rojviroon T, Rojviroon O, Sirivithayapakorn S, Angthong S (2021) Application of TiO2 nanotubes as photocatalysts for decolorization of synthetic dye wastewater. Water Resour Ind 26:100163. https://doi.org/10.1016/j.wri.2021.100163

11. Li B et al (2021) Porous g-C3N4/TiO2 S-scheme heterojunction photocatalyst for visible-light driven H2-production and simultaneous wastewater purification. Int J Hydrogen Energy 46(64):32413–32424. https://doi.org/10.1016/j.ijhydene.2021.07.090

12. Xu Q, Zhang L, Cheng B, Fan J, Yu J (2020) S-Scheme Heterojunction Photocatalyst. Chem 6(7):1543–1559. https://doi.org/10.1016/j.chempr.2020.06.010

13. Manna S, Remya N, Singhal N (2023) Advancements in S-scheme photocatalytic material for wastewater treatment. J Environ Chem Eng 11(3):109838. https://doi.org/10.1016/j.jece.2023.109838

14. Li Y, Zhou M, Cheng B, Shao Y (2020) Recent advances in g-C3N4-based heterojunction photocatalysts. J Mater Sci Technol 56:1–17. https://doi.org/10.1016/j.jmst.2020.04.028

15. Chen P, Di S, Qiu X, Zhu S (2021) One-step synthesis of F-TiO2/g-C3N4 heterojunction as highly efficient visible-light-active catalysts for tetrabromobisphenol A and sulfamethazine degradation. Appl Surf Sci 587:152889. https://doi.org/10.1016/J.APSUSC.2022.152889

16 Remya N, Swain A (2019) Soft drink industry wastewater treatment in microwave photocatalytic system – Exploration of removal efficiency and degradation mechanism. Sep Purif Technol 210:600–607. https://doi.org/10.1016/j.seppur.2018.08.051

17. Shukla N, Sahoo D, Remya N (2019) Biochar from microwave pyrolysis of rice husk for tertiary wastewater treatment and soil nourishment. J. Clean. Prod. 235:1073–1079. https://doi.org/10.1016/j.jclepro.2019.07.042

18. Neha S, Rajput P, Remya N (2022) Biochar from microwave co-pyrolysis of food waste and polyethylene using different microwave susceptors – Production, modification and application for metformin removal. Environ Res 210:112922. https://doi.org/10.1016/j.envres.2022.112922

19. Narde SR, Remya N (2022) Biochar production from agricultural biomass through microwave-assisted pyrolysis: predictive modelling and experimental validation of biochar yield. Environ. Dev. Sustain. 24(9):11089–11102. https://doi.org/10.1007/s10668-021-01898-9

20. Sudarsh A, Remya N, Swain A (2023) Recent research advancements in microwave photocatalytic treatment of aqueous solutions. Environ Monit Assess 195:142. https://doi.org/10.1007/s10661-022-10604-9

21 Bhavani P, Hussain M, Park YK (2022) Recent advancements on the sustainable biochar based semiconducting materials for photocatalytic applications: A state of the art review. J Clean Prod 330:129899. https://doi.org/10.1016/j.jclepro.2021.129899

22 Wang J et al (2023) Construction of tubular g-C3N4/TiO2 S-scheme photocatalyst for high-efficiency degradation of organic pollutants under visible light. J. Alloys Compd 947:169659. https://doi.org/10.1016/j.jallcom.2023.169659

23. Alothman AA et al (2022) Facile synthesis and comparative study of the enhanced photocatalytic degradation of two selected dyes by TiO2-g-C3N4 composite. Environ Sci Pollut Res 30:37332–37343. https://doi.org/10.1007/s11356-022-24839-z